SMAR 2015 – Third Conference on Smart Monitoring,
Assessment and Rehabilitation of Civil Structures

SMAR 2015

Behavior of Concrete-Filled Fiber Tubes with Large Deformable FRP under Axial Compressive Loading

Omar I. Abdelkarim[1], and Mohamed A. ElGawady[2]

[1] Ph.D. Candidate, Missouri University of Science and Technology, Rolla, MO, USA
[2] Benavides Associate Professor, Missouri University of Science and Technology, Rolla, MO, USA

ABSTRACT: This paper investigates experimentally and numerically the behavior of the concrete-filled fiber tubes using large deformable fiber reinforced polymer (FRP) under axial compressive loading. Two types of large deformable FRP were used in this paper; large rupture strain FRP (LRS-FRP) and FRP made with fibers oriented with ± 45°. The finite element (FE) analysis was conducted using LS-DYNA software. The LRS-FRP is made with polyethylene naphthalate (PEN) and polyethylene terephthalate (PET) fibers. The PEN and PET fibers are environmentally friendly as they are made from recycled materials (e.g. bottles). They have high ultimate strain (> 5.0%) however their elastic modulus is low. The experimental work examined the behavior of the CFFT made with fibers oriented with ± 45 and the FE study examined the CFFT made with LRS-FRP. The experimental work consisted of two CFFT cylinders had outer three layered FRP tube with fibers oriented at ± 45° and one CFFT cylinder has three hybrid-layered FRP [± 45/0]. The investigated cylinders were tested under axial cyclic compressive loading. The FE study investigated six cylinders of PET-FRP and three cylinders of PEN-FRP under axial compressive loading. The experimental results presented in this paper indicated that the FRP made with fibers oriented with ± 45° has ability to achieve a good ductility. The fibers oriented with ± 45° were reorienting during loading before reaching the rupture strain without considerable enhancement in the compressive strength. The FE results showed that the thick LRS-FRP achieved much better behavior in strength and ductility than the conventional FRP. This result indicated that the FRP ultimate strain had a great effect on the concrete confinement even if the elastic modulus was low.

1 INTRODUCTION

The use of fiber-reinforced polymer (FRP) has grown rapidly in the past two decades. The main purpose of using FRP is to enhance the strength and ductility of a structural member. FRP tubes confine the concrete structural element and in turn increase its compressive strength. Concrete-filled fiber tubes (CFFTs) have many advantages such as light weight-to-strength ratio, high confinement and corrosion resistance compared to steel tubes. Seismic behavior of CFFT columns has been studied (e.g. ElGawady and Sha'lan 2011; Carter et al. 2014).

Au and Buyukozturk (2005) investigated the effect of fiber orientation on the confinement in CFFT cylinders. It was concluded that the angle fiber jackets showed a ductile failure modes with fiber reorientation mechanism. By this mechanism the fiber reoriented during loading

which dissipating a high energy before reaching fiber rupture without considerable strength enhancement.

The most common FRP composites are made with carbon (CFRP), glass (GFRP), and aramid (AFRP). Such composites have linear elastic stress-strain relations with a rupture failure strain ranged around 1.5% to 2.5%. Recently, new FRP composites have been introduced as alternatives to the common FRP. These composites are made of polyethylene terephthalate (PET) and polyethylene naphthalate (PEN) fibers. However such composites have low elastic modulus, they have large rupture strains (LRS) usually larger than 5.0%. PET-FRP and PEN-FRP are usually made from recycled bottles. Therefore, they are much cheaper than the conventional FRP. Recently, some experimental works have been conducted to investigate the performance of LRS-FRP for jacketing concrete columns (Dai et al. 2011). These researches have shown that the columns reached the ultimate state without FRP rupture.

This paper is primarily concerned with the behavior of the CFFT columns wrapped with large deformable FRP under axial compressive loading and their finite element (FE) modeling. The paper started with investigating experimentally the behavior of the CFFT made with fibers oriented with ± 45° and fibers oriented with ± 45°/0. Then, the FE study examined numerically the behavior of the CFFT made with LRS-FRP. The validation of the FE model will be conducted with the experimental work.

2 EXPERIMENTAL WORK

2.1 Test specimens

Three CFFTs were investigated during the course of this research (see Table 1). Two CFFT cylinders (CFFT-1 & CFFT-2) had outer three layered FRP tube with fiber oriented at ± 45°. CFFT-1 cylinder was prepared with carbon fiber (CFRP) and CFFT-2 cylinder was prepared with glass fiber (GFRP). The CFFT-3 cylinder had three hybrid-layered GFRP tube [± 45°/± 45°/0°]. All specimens were tested under axial cyclic compressive loading.

The specimens had an outer diameter of 210 mm and a height of 406 mm. The FRP tubes of the CFFTs were prepared manually by a wet-layup process on sonotube and were used as a mold for concrete pouring. The last wrapped layer of FRP tube was provided with 30% overlap to prevent premature debonding failure. The studied parameters were the effect of fiber orientation on the overall strength and ductility of CFFT cylinders.

2.2 Material properties

The average cylindrical concrete compressive strength (f_c') at 56 days was 55.1 MPa. The properties of the FRP were referenced based on the manufacturer data sheet of Tyfo® BCC and Tyfo® BC of FRP tubes oriented at ± 45° and Tyfo® SHE-51 of unidirectional FRP tube. The manufacturer tensile strength, Young's modulus, and maximum elongation of GFRP laminate oriented at ± 45° based on a nominal thickness of 0.86 mm are 280.0 MPa, 18.6 GPa and 1.50 %, respectively. The manufacturer tensile strength, Young's modulus, and maximum elongation of CFRP laminate oriented at ± 45° based on a nominal thickness of 0.86 mm are 661.0 MPa, 48.0 GPa, and 1.40 %, respectively. The manufacturer tensile strength, Young's modulus and maximum elongation of unidirectional GFRP laminate based on a nominal thickness of 1.25 mm are 575.0 MPa, 26.1 GPa, and 2.20%, respectively.

Table 1: Specimens descriptions

Specimen number	FRP tube	Outer diameter (mm)	Concrete cylindrical strength f_c' (MPa)
CFFT-1	CFRP- Three ± 45° layers		
CFFT-2	GFRP- Three ± 45° layers	210	55.1
CFFT-3	GFRP- Two ± 45° layers + one 0° layer		

2.3 Test set-up and loading protocol

Compression tests were carried out using MTS machine with a loading rate of 0.5 mm/min. All test data, including the strains, loads, and displacements, were recorded simultaneously using a data acquisition system. Two horizontal and two vertical strain gauges were installed on the outer surface at the mid-height of the FRP tube. In addition, two string potentiometers were attached on the outer surface of the FRP tube to obtain the axial deformation of the middle region of 140 mm for each specimen. All specimens were tested under compression loading on cyclic scheme. The cyclic compression involved full loading/unloading cycles, where the unloading of each cycle was designed to terminate at a 0.5 kN (near zero) and the reloading of each cycle was designed to terminate at the unloading displacement of the same cycle. The loading scheme followed nine steps started at axial strain of 0.125 % and was increased gradually until failure of the specimen. Each loading step repeated three cycles.

3 EXPERIMENTAL RESULTS AND DISCUSSION

The backbone axial strain-load curves of the cyclic curves of all specimens are shown in Fig. 1(a). All specimens had almost the same initial stiffness up to load level of 1,820 kN. It was worthy noted that the cylinders with FRP tubes oriented at ± 45° (CFFT-1 and CFFT-2) had only one slope up to the ultimate load. The reason for that was the effect of the 45^o FRP. The angle-ply FRP has an ability to give high ductility by the reorientation phenomenon (Au and Buyukozturk 2005). Under axial loading, the angle-ply fiber reoriented from the initial case ($\pm$45) toward the hoop direction. Therefore, CFFT-1 cylinder reached to the ultimate load of 1,833 kN without fiber rupture. It can be noted also in Fig. 1(a) that the load started to increase after axial strain of 6.0% in CFFT-1 which means the fibers were reoriented to close to the hoop direction. However, CFFT-2 cylinder achieved higher axial capacity of 1,967 kN, it was ruptured earlier than CFFT-1 at axial strain of 4.0%. It can be concluded that the GFRP was reorienting faster than the CFRP hence the fibers were much closer to the hoop direction after the reorientation. That explained also why CFFT-2 achieved higher capacity than CFFT-1.

CFFT-3 cylinder with hybrid FRP tube, fiber orientations were ± 45°/0, had a different behavior than CFFT-1 and CFFT-2. It had two slopes before reaching the ultimate capacity of 2,029 kN. The strength dropped suddenly to 1,332 kN after reaching the ultimate axial capacity because of rupture of some parts of unidirectional fibers. The strength was gradually decreased up to full rupture of the FRP tubes at ultimate axial strain of 7.0%. It was clear in Fig. 1(a) that CFFT-3 cylinder had better overall behavior in strength. However, CFFT-3 had higher strength than CFFT-1 cylinder, CFFT-1 cylinder had considerable higher ductility. Figs. 1(b), 1(c), and 1(d) show the failure modes of the tested cylinders. Table 2 summarizes the experimental results of

the tested cylinders. The confined concrete (f'_{cc}) strengths and their ratio to the unconfined concrete strength (f'_c) are summarized in Table 2.

Table 2: Experimental results of tested cylinders

Specimen number	Axial capacity (kN)	Ultimate axial strain	f'_{cc} (MPa)	f'_{cc} / f'_c	FRP rupture
CFFT-1	1,837	12.0	53.0	0.97	No
CFFT-2	1,971	4.0	57.0	1.04	Yes
CFFT-3	2,033	7.0	59.0	1.07	Yes

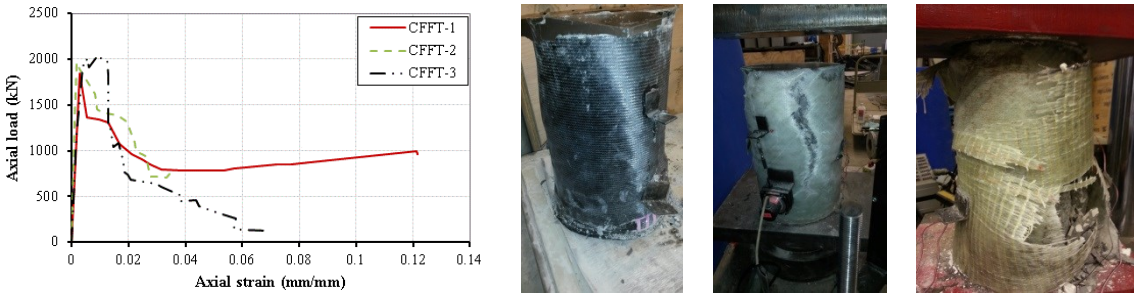

(a) (b) (c) (d)

Figure 1. (a) axial strain-axial load relationship, (b) mode of failure of CFFT-1, (c) mode of failure of CFFT-2, and (d) mode of failure of CFFT-2

4 FINITE ELMENT ANALYSIS

The purpose of the FE study in this research is to investigate the performance of the new FRP category (PET and PEN) comparable to the conventional FRP (GFRP and CFRP). PET-600, PET-900, and PEN-600 were investigated in this study. The difference between the type of 600 and the type of 900 is only the sheet thickness. One, two, and three layers were studied for each type. The PET-600 and PEN-600 sheet thicknesses of one, two, and three layers are 0.86 mm, 1.7 mm, and 2.5 mm, respectively. The PET-900 sheet thicknesses of one, two, and three layers are 1.25 mm, 2.5 mm, and 3.8 mm, respectively. Table 3 summarizes the variables of the investigated cylinders.

Table 3: Summary of cylinders variables (Modified from Dai et al. 2011, © ASCE)

Specimen number	FRP type	Total thickness (mm)	No. of layers
PEN-600-I		0.86	One
PEN-600-II	PEN-600	1.70	Two
PEN-600-III		2.50	Three
PET-600-I		0.86	One
PET-600-II	PET-600	1.70	Two
PET-600-III		2.50	Three
PET-900-I		1.25	One
PET-900-II	PET-900	2.50	Two
PET-900-III		3.80	Three

4.1 Geometry

The cylinders under consideration in this study were investigated numerically under monotonic axial load with displacement control in LS-DYNA software. Each cylinder had a circular cross-section with an outer diameter of 210 mm and a height of 406 mm inserted between two rigid cubic steel plates with dimensions 230 mm x 230 mm x 50 mm (see Fig. 2). The concrete cylinder and steel plates were modeled using solid elements. The outer FRP tube was simulated using shell elements. All solid elements were modeled with constant-stress and one-point quadrature to reduce the computational time. Hourglass control was used to avoid spurious singular modes (i.e., hourglass modes) for solid elements. The hourglass value for all models was taken as the default value of 0.10. Contact elements surface-to-surface were used to simulate the interface between the concrete cylinder and the outer FRP tube. Node-to-surface contact elements were used between the rigid plates and the cylinder (the concrete cylinder and the FRP tube).

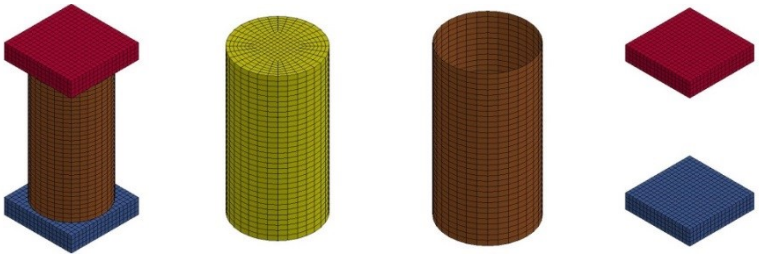

(a) (b) (c) (d)

Figure 2. Finite element model components: (a) 3-D view, (b) concrete cylinder, (c) FRP tube, (d) top and bottom rigid plates

4.2 Concrete material model

Different material models are available in LS-DYNA to simulate concrete materials. Because the Karagozian and Case Concrete Damage Model Release 3 (K&C model) exhibited good agreement with the experimental results in collected previous studies, it was chosen for this study (Abdelkarim and ElGawady 2014b). The model was developed based on the theory of plasticity. The model has three shear failure surfaces: yield, maximum, and residual (Malvar et al. 1997). This material model has eighty parameters that can be either user defined or automatically generated. This paper used the automatic generation option, with f_c' being the main input to the model.

4.3 FRP material model

FRP material was modeled as an orthotropic material using "108-ortho_elastic_plastic" material. This model combines orthotropic elastic plastic behavior for shells only. This material is defined by the engineering constants: elastic modulus (E1), tangent modulus (E2), shear modulus (G), and poisson's ratio (PR), in the two principle axes (a and b). Additionally, the fiber orientation is defined by a vector. Failure criterion for FRP was defined using "000-add_erosion," by assigning the ultimate strain of FRP in "EFFEPS" card.

The material properties of PET-FRP and PEN-FRP composites have been studied by Dai et al. (2011). Such types of FRP have an approximately bilinear stress-strain relationships can be described in terms of two modulus of elasticity namely the initial elastic modulus (E1) and the tangent modulus (E2), tensile strength and rupture strain. The material properties of PET-FRP and PEN-FRP are summarized in Table 4.

Table 4: Material properties of new FRP category (reproduced after Dai et al. 2011 ©ASCE)

FRP Type	E1 (GPa)	E2 (GPa)	Tensile strength (MPa)	Rupture strain (%)
PET-FRP	17.9	8.3	750	8.71
PEN-FRP	27.0	12.0	760	6.26

4.4 Boundary conditions and loading

Displacements and rotations in all directions were prevented at the bottom of the bottom plate. Monotonic downward displacement loading was applied on the top plate for axial compressive loading until failure occurred. This failure was defined as the rupture of the FRP or the crushing of the concrete cylinder.

5 RESULTS AND DISCUSSIONS

5.1 Model validation

In order to validate the FE model, numerical analysis was conducted for CFFT-3 cylinder and was compared to the experimental results. The axial strain was obtained by dividing the axial displacement by the cylinder height (406 mm). The axial load applied on the cylinder was obtained from FE analysis by summation of the vertical reactions at the bottom plate. The axial strain versus the axial load from the experimental cyclic test and the FE monotonic numerical analysis are plotted in Fig. 3(a). The FE model, in general, was able to capture the behavior of the tested cylinder up to the maximum load. The initial stiffness in the FE was very close to the experimental up to a load level about 1,555 kN. The axial capacity of CFFT-3 were 2,029 kN and 2,042 kN during the experimental work and the FE analysis, respectively. The difference between the experimental strength and the FE strength was 0.66 %. The error is calculated as the absolute value of the difference between the experimental and the FE ultimate load divided by the experimental ultimate load. The ultimate axial strain of the tested cylinder was 0.07 and 0.017 during the experimental work and the FE analysis, respectively. The big difference between the ultimate axial strains experimentally and in the FE analysis was because the FE could not capture the reorientation of the angle-ply fibers (45^o). However, this weakness of the FE model will not affect studying the LRS-FRP as they will be unidirectional fibers. The FE showed that the maximum FRP hoop strain at the mid height which matched the experimental behavior as the first FRP rupture was at the mid height (Fig. 3(b)). FE results showed a very good agreement with mode of failure comparable to the experimental results (Fig. 3(c) & (d)).

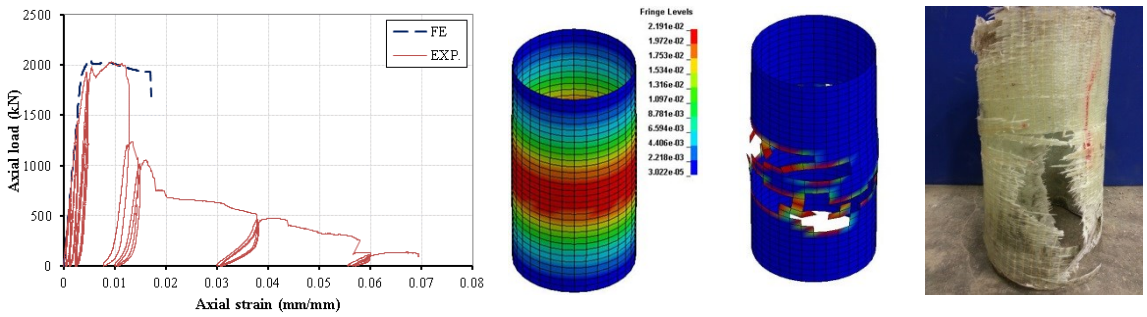

(a) (b) (c) (d)

Figure 3. (a) Axial strain-axial load of the experimental and FE results, (b) FRP hoop strains during FE, (c) FRP rupture during FE and (d) FRP rupture during experimental

5.2 LRS-FRP FE results

All investigated cylinders, whether with PET or PEN fibers, were failed by FRP rupture. The ultimate axial capacity of PEN-I, II, and III were 2,000 kN, 2,287 kN, and 3,000 kN, respectively and with ultimate axial strains of 5.1%, 5.2%, and 5.4%, respectively (Fig. 4). The ultimate axial capacity of PET600-I, II and III were 1,980 kN, 2,029 kN, and 2,722 kN, respectively and with ultimate axial strains of 6.9%, 6.8% and 7.0%, respectively (Fig. 4). The ultimate axial capacity of PET900-I, II and III were 2,000 kN, 2,691 kN, and 3,468 kN, respectively and with ultimate axial strains of 6.8%, 6.9%, and 7.2%, respectively (Fig. 4). Table 5 summarizes the FE results. The confined concrete (f'_{cc}) strengths and their ratio to the unconfined concrete strength (f'_c) are summarized in Table 5.

Table 5: Summary of FE results

Specimen number	Ultimate axial load (kN)	Ultimate axial strain (%)	f'_{cc} (MPa)	f'_{cc} / f'_c
PEN-600-I	2,000	5.1	58.2	1.05
PEN-600-II	2,287	5.2	66.4	1.20
PEN-600-III	3,000	5.4	87.2	1.58
PET-600-I	1,980	6.9	57.5	1.04
PET-600-II	2,029	6.8	59.0	1.07
PET-600-III	2,722	7.0	79.1	1.43
PET-900-I	2,000	6.8	58.2	1.05
PET-900-II	2,691	6.9	78.2	1.42
PET-900-III	3,468	7.2	100.8	1.83

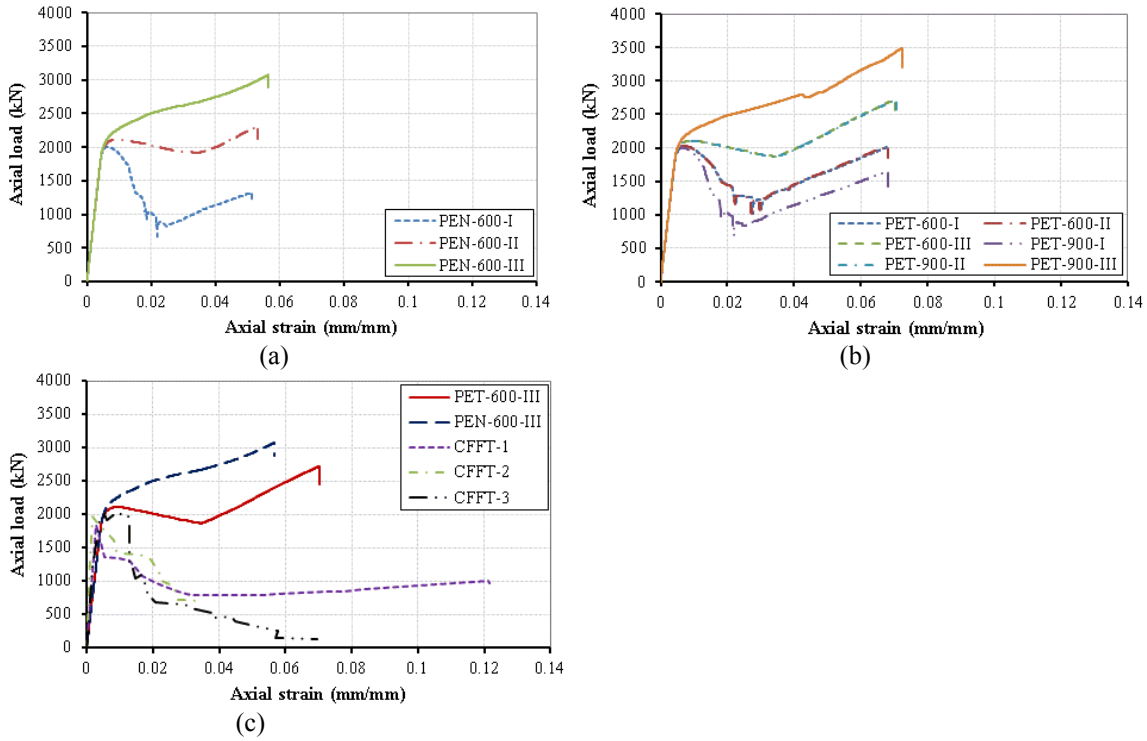

Figure 4. Axial strain-axial load of cylinders with: (a) PEN-FRP, (b) PET-FRP, and (c) PET-600-III, PEN-600-III, CFFT-1, CFFT-2, and CFFT-3

It was clear that all investigated cylinders had the same initial stiffness. It was worthy noted that the axial strain-axial load of PEN-600-III and PET-900-III had a bi-increasing relation, however all other cylinders behaved with increasing-decreasing relation. The strength of all cylinders except PEN-600-III and PET-900-III returned to increase after decreasing. It was noted from Figs. 4(a) and 4(b) that PET-FRP gave a higher ductility than the PEN-FRP. Fig. 4(c) illustrates a comparison between the experimental results of using fibers oriented with ± 45° and the finite element results of using LRS (600)-FRP of three layers. It was noted that the higher strength could be achieved using PEN-FRP however the higher ductility could be achieved using CFRP oriented at ± 45°. The CFFT-3, with hybrid fibers, and PET-600-III had the same axial strain but PET-600-III had around 34% higher strength. In general, the cylinders with thick LRS-FRP achieved much better behavior than the conventional FRP. This indicated that the FRP ultimate strain had a great effect on the concrete confinement even if the elastic modulus was low.

6 CONCLUSIONS

This paper presented the behavior of the concrete-filled fiber tubes using large deformable FRP under axial compressive loading during experimental and numerical studies. Two types of large deformable FRP were used in this paper; large rupture strain FRP (LRS-FRP) and FRP made with fibers oriented with ± 45°. The finite element (FE) analysis was conducted using LS-DYNA software. The results demonstrated that the cylinders confined by fibers oriented with ± 45° have an ability to dissipate energy by the mechanism of fiber reorientation. The bad effect of this mechanism is the very low enhancement on the compressive strength. Generally, the cylinders confined with LRS-FRP have a better performance in strength and ductility than the cylinders confined with conventional FRP (glass and carbon) especially if LRS-FRP was thick. The ultimate strain had a considerable effect on the concrete confinement.

7 ACKNOWLEDGEMENT

This research was conducted by Missouri University of Science and Technology and was supported by Missouri Department of Transportation (MoDOT) and the National University Transportation Center (NUTC) at Missouri University of Science and Technology (Missouri S&T). However, any opinions, findings, conclusions, and recommendations presented in this paper are those of the authors and do not necessarily reflect the views of the sponsors.

REFERENCES

Abdelkarim, O. and ElGawady, M. (2014a). “Behavior of Hybrid FRP-Concrete-Steel Double-Skin Tubes Subjected to Cyclic Axial Compression.” Structures Congress 2014: pp. 1002-1013.

Abdelkarim, O. and ElGawady, M. (2014b). "Analytical and Finite-Element Modeling of FRP-Concrete-Steel Double-Skin Tubular Columns." J. Bridge Eng., 10.1061/(ASCE)BE.1943-5592.0000700 , B4014005.

Au, C. and Buyukozturk, O. (2005). ”Effect of Fiber Orientation and Ply Mix on Fiber Reinforced Polymer-Confined Concrete.” J. Compos. Constr., 9(5), 397–407.

Carter, J., Abdelkarim, O., ElGawady, M., and Khayat, K. (2014). “FRP Confinement of High Strength Self-Consolidating Concrete.” 10th U.S. National Conf. on Earthquake Engineering, Alaska, USA.

Dai, J., Bai, Y., and Teng, J. (2011). ”Behavior and Modeling of Concrete Confined with FRP Composites of Large Deformability.” J. Compos. Constr., 15(6), 963–973.

ElGawady, M. and Sha’lan, A. (2011). ”Seismic Behavior of Self-Centering Precast Segmental Bridge Bents.” J. Bridge Eng., 16(3), 328–339.